Nootkatone attenuates oxidative stress, focal adhesion abundance, and profibrotic gene expression in human keloid fibroblasts

Running title：Nootkatone in human keloid fibroblasts

Abstract

Introduction. Keloids are driven by persistent fibroblast activation characterized by excessive matrix deposition, abnormal motility, and oxidative/inflammatory signaling. Nootkatone, a natural sesquiterpenoid present in grapefruit, has reported antioxidant and anti-inflammatory activities, but its effects on human keloid fibroblasts (HKFs) remain unclear.

Material and methods. SV40-immortalized HKFs and non-keloid HSFs were exposed to nootkatone. Dose-response analysis showed that HKFs were more sensitive to nootkatone than HSFs; therefore, 20 and 40 μg/mL nootkatone (hereafter termed NKT20 and NKT40, respectively) were selected for subsequent HKF-focused assays, including wound closure, Transwell invasion, immunofluorescence analyses of F-actin organization, α-SMA, vinculin-positive focal adhesions, and intracellular reactive oxygen species (ROS), as well as RT-qPCR assays for extracellular matrix- and inflammation-related genes.

Results. HKFs were more sensitive to nootkatone than HSFs in the viability assay. Nootkatone reduced scratch-wound closure and Transwell invasion, decreased phalloidin signal, cell aspect ratio, α-SMA intensity, vinculin-positive focal adhesion counts, and intracellular ROS. NKT20 reduced the mRNA expression of COL1A1, COL3A1, and FN1, whereas NKT20 and NKT40 reduced IL8 and HMGB1.

Conclusions. Nootkatone attenuated multiple profibrotic features in an SV40-immortalized HKF model, including motility-associated readouts, cytoskeletal organization, focal adhesion abundance, oxidative stress, and extracellular matrix/inflammatory gene expression. These findings support further mechanistic evaluation of nootkatone in primary, non-immortalized, multi-donor keloid fibroblast models.

Keywords: nootkatone; keloid fibroblast; oxidative stress; focal adhesion; α-SMA; extracellular matrix

Introduction

Fibroblasts are central regulators of cutaneous homeostasis, wound repair, and extracellular matrix (ECM) remodeling. In normal skin, they maintain dermal architecture and respond to biochemical and mechanical cues. After injury, they proliferate, migrate into the wound bed, and can differentiate into contractile myofibroblasts characterized by α-smooth muscle actin (α-SMA) expression [1-3]. When this activation becomes persistent or dysregulated, pathological scarring and fibrosis may develop, including keloids, which are marked by excessive collagen

deposition, altered mechanics, chronic inflammation, and an exaggerated myofibroblast phenotype [4-7].

Oxidative stress is increasingly recognized as an upstream amplifier of fibroblast activation. Excess reactive oxygen species (ROS) can enhance fibroblast survival, motility, and matrix remodeling while also promoting the expression or release of inflammatory mediators [8-10]. In fibrotic or inflammatory wound environments, IL8 can support fibroblast-associated invasive behavior and matrix-remodeling programs, whereas HMGB1 released from stressed cells can further reinforce profibrotic signaling [11,12].

Fibroblast migration depends on coordinated actin remodeling, front–rear polarity, and focal adhesion turnover. Focal adhesions couple ECM engagement to intracellular force transmission, and vinculin is a key structural component that links the integrin-talin complex to actin filaments [13-16]. In activated fibroblasts, reinforcement of stress fibers, increased focal adhesion formation, and enhanced matrix synthesis collectively support tissue contraction and scar maturation [1,4,7,17].

Nootkatone (NKT), a naturally occurring sesquiterpenoid enriched in grapefruit, has emerged as a bioactive compound with antioxidant and anti-inflammatory effects in several experimental systems [18-22]. Mechanistically, previous studies have linked NKT to NQO1/AMPK-associated anti-inflammatory signaling, inhibition of NF-κB activation, activation of Nrf2/HO-1 signaling, and suppression of ROS-dependent NLRP3 inflammasome activation [18-22]. These pathways provide a rationale for testing NKT in HKFs because redox imbalance and inflammatory amplification are closely coupled to fibroblast activation and matrix remodeling in keloid biology. However, its influence on keloid fibroblast behavior has not been defined. Given the importance of oxidative stress, cell motility, focal adhesion dynamics, and ECM deposition in keloid biology, we investigated whether NKT could restrain human keloid fibroblast activation. Using viability assays, motility assays, immunofluorescence phenotyping, ROS imaging, and targeted RT-qPCR, we examined how NKT affects viability, wound closure, invasion, cytoskeletal organization, focal adhesion abundance, inflammatory gene expression, and ECM-related transcription in HKFs.

Materials and Methods

Cell culture and nootkatone treatment

Human keloid fibroblasts (HKFs) and non-keloid human skin fibroblasts (HSFs) were obtained from Shanghai Jinyuan Biotech, China. According to the cell-bank documentation, the HSF model was an SV40-immortalized fibroblast cell line derived from skin tissue of a middle-aged male donor and established in 2009 by the Kunming Cell Bank, Chinese Academy of Sciences, through lentiviral transduction carrying the SV40 gene; HSFs were used at passage 4 in this study. The HKF model was an SV40-immortalized fibroblast cell line generated from fibroblasts cultured from surgically excised keloid tissue of a middle-aged male donor through lentiviral transduction carrying the SV40 gene. Both cell models tested negative for mycoplasma

contamination before experiments. Within each experiment, control and NKT-treated cells were prepared from the same cell model and passage to minimize intra-experimental passage-related variation. Cells were maintained in Dulbecco's modified Eagle medium (DMEM; Procell, Wuhan, China) supplemented with fetal bovine serum (FBS; Gibco, Brazil) under humidified conditions (37°C, 5% CO_2). Nootkatone (NKT; CAS: 4674-50-4; Acmec, Shanghai, China) was dissolved in DMSO to prepare a stock solution and diluted into culture medium before use. The final DMSO concentration was kept constant across groups. A concentration-response experiment was first performed in HKFs and HSFs. Based on the HKF viability curve, two working concentrations, 20 and 40 μg/mL nootkatone, were selected for subsequent experiments and are referred to as NKT20 and NKT40, respectively.

Cell viability assay

HKFs and HSFs were seeded into 96-well plates at a density of 2000 cells per well and allowed to adhere overnight. Cells were then treated with the indicated concentrations of NKT for 48 h before Cell Counting Kit-8 reagent (Glpbio, Shanghai, China) was added according to the manufacturer's instructions. After 3 h, absorbance was read at 450 nm using a microplate reader. HSFs were included in the concentration-response viability assay as a non-keloid comparator for concentration selection; subsequent functional and molecular assays were limited to HKFs because the primary aim was to characterize modulation of the keloid fibroblast activation phenotype.

Wound healing and Transwell invasion assays

For the wound-healing assay, HKFs were cultured to near confluence in 6-well plates, and a uniform wound was created using a sterile 1-mL pipette tip (Jet Biotech, Guangzhou, China). Detached cells were removed by PBS washing, and serum-free DMEM containing vehicle, NKT20, or NKT40 was added. Images were captured at 0 and 48 h after scratching under an inverted microscope (Nikon, Tokyo, Japan). Wound closure was quantified in ImageJ as the percentage reduction in wound area relative to the 0-h time point. No proliferation blocker was used during scratch closure; therefore, wound closure was interpreted as a composite endpoint that may include migration, proliferation, and survival effects.

For the Transwell invasion assay, inserts with 8-μm pores (Jet) were pre-coated with Matrigel (Servicebio, Wuhan, China). Cells were seeded into the upper chamber in serum-free medium, with complete medium in the lower chamber as a chemoattractant. After the invasion period, non-migrated cells were removed, and invaded cells were fixed, crystal violet-stained, imaged, and counted in multiple random microscopic fields at 200× magnification.

Immunofluorescence staining and image analysis

For α-SMA/phalloidin staining, HKFs were seeded in 24-well plates and treated with vehicle, NKT20, or NKT40. Cells were fixed with paraformaldehyde, permeabilized, and blocked before incubation with an anti-α-SMA primary antibody (1:1000, ET1607-53, Huabio, Hangzhou, China) and the corresponding goat anti-rabbit IgG H&L secondary antibody (1:1000, HA1121,

Huabio). F-actin was labeled with fluorescent phalloidin (CA1610, Solarbio, Beijing, China), and nuclei were counterstained with DAPI (Servicebio). For vinculin staining, cells were processed similarly using an anti-vinculin antibody (1:1000, ET1705-94, Huabio) and DAPI. No-primary-antibody controls were included for the α-SMA and vinculin immunofluorescence assays by omitting the primary antibody while retaining the corresponding secondary antibody and all subsequent staining, washing, mounting, and imaging steps. No-primary controls were imaged using the same exposure settings as the corresponding experimental samples and were used to assess nonspecific secondary-antibody/background fluorescence before quantitative image analysis. All images used for quantitative comparison were acquired with identical exposure settings within the same experiment. Image analysis was performed in ImageJ. For Fig. 3, integrated F-actin intensity, cell aspect ratio, and α-SMA mean fluorescence intensity (MFI) per cell were quantified from at least five independent fields per group. For Fig. 4, vinculin-positive focal adhesions were segmented after background subtraction and thresholding, and focal adhesion counts per cell were quantified in ImageJ.

ROS measurement

Intracellular ROS was assessed using DCFH-DA (Servicebio). HKFs were treated with vehicle, NKT20, or NKT40 for 24 h and then incubated with DCFH-DA in serum-free medium in the dark at 37°C for 40 min. After washing, fluorescence and phase-contrast images were captured using identical settings. Mean gray values were quantified in ImageJ.

Total RNA was isolated using Beyozol kit（Beyotime,Shanghai,China） and reverse transcribed using the First Strand cDNA Synthesis Kit(Beyotime) . SYBR Green qPCR Mix (Beyotime) was used to perform qPCR assays. Relative gene expression was calculated by the 2^-ΔΔCt method using GAPDH as the internal reference. Primer sequences used in the present study are listed in Table 1.

Table 1. Primer sequences used for RT-qPCR.

Target gene	Forward primer (5′–3′)	Reverse primer (5′–3′)
COL1A1	GAGGGCCAAGACGAAGACATC	CAGATCACGTCATCGCACAAC
COL3A1	GGAGCTGGCTACTTCTCGC	GGGAACATCCTCCTTCAACAG
FN1	CAAATGGTTCAGCCCCAGTCC	GTCCGCTCCCACTGTTGATTTATC
IL8	GTGGTGGCAGATGTGCTTAG	TTCAGAGCCACAAACAAGGC
HMGB1	TGTGCAAACTTGTCGGGAG	TCTTCATAACGGGCCTTGTC
GAPDH	AGAAGGCTGGGGCTCATTTG	AGGGGCCATCCACAGTCTTC

Statistical analysis

Data are presented as mean ± SD. Comparisons between two groups were performed using the unpaired Student's t-test, whereas comparisons involving more than two groups were analyzed by one-way ANOVA followed by an appropriate post hoc test. Graphing and statistical analyses were performed in GraphPad Prism 10 (GraphPad Software, San Diego, CA, USA). A p-value < 0.05 was considered statistically significant. Unless otherwise stated, n represents independent experimental repeats or quantified microscopic fields rather than independent donor-derived fibroblast lines.

Results

Nootkatone reduces HKF viability and alters cell morphology more prominently than in HSFs

Dose-response analysis in these SV40-immortalized fibroblast models showed that nootkatone reduced HKF viability across the tested range, with significant decreases emerging at intermediate concentrations and more pronounced inhibition at the highest concentrations (Fig. 1A). HSFs were less sensitive under the same conditions and showed only a modest reduction at the upper end of the concentration range (Fig. 1B). Representative phase-contrast images of HKFs showed progressively reduced cell spreading, a more contracted morphology, and lower cell density with increasing NKT exposure (Fig. 1C). On the basis of this response profile, NKT20 and NKT40 were selected for subsequent experiments.

Nootkatone reduces wound closure and invasion of HKFs

Both NKT20 and NKT40 slowed closure of the scratch area relative to control cells in the wound-healing assay (Fig. 2A,B). The inhibitory effect was more pronounced in the NKT40 group. Consistent with this finding, Transwell assays showed fewer invaded cells in both NKT-treated groups than in the control group, with the lowest number observed after NKT40

treatment (Fig. 2C,D). These data indicate that NKT impaired both wound closure and invasive behavior of HKFs.

Nootkatone attenuates actin organization and lowers α-SMA expression

Triple immunofluorescence staining revealed prominent phalloidin-labeled actin stress fibers and strong α-SMA signal in control HKFs, whereas both signals were visibly reduced after NKT treatment (Fig. 3A). Quantitative image analysis demonstrated that integrated phalloidin intensity was significantly lower in NKT20- and NKT40-treated cells (Fig. 3B). Cell aspect ratio was also reduced after NKT exposure (Fig. 3C), consistent with a less elongated morphology. In addition, α-SMA mean fluorescence intensity per cell decreased significantly in both treatment groups (Fig. 3D), supporting attenuation of the activated myofibroblast-like phenotype.

Nootkatone reduces ECM-related gene expression

To determine whether the structural changes induced by NKT were accompanied by altered profibrotic transcription, COL1A1, COL3A1, and FN1 mRNA levels were measured in control and NKT20-treated HKFs. All three transcripts were significantly reduced in the NKT20 group, with the largest decreases observed for COL1A1 and COL3A1 and a more moderate reduction in FN1 (Fig. 3E-G). These results indicate that NKT20 suppressed ECM-related gene expression under the conditions tested.

Nootkatone reduces vinculin-positive focal adhesion abundance

Focal adhesions are required for force transmission and persistent migration. Vinculin immunofluorescence was therefore used to assess adhesion-related structures after NKT exposure. Control HKFs displayed abundant punctate vinculin-positive focal adhesions, whereas both NKT20 and NKT40 reduced the number of detectable focal adhesions per cell (Fig. 4A,B). This change is consistent with the reduced migratory and invasive behavior observed in Fig. 2.

Nootkatone lowers intracellular ROS and inflammatory gene expression

DCFH-DA staining showed strong intracellular ROS-associated fluorescence in control HKFs, whereas both NKT20 and NKT40 substantially reduced the signal (Fig. 5A,B). RT-qPCR further showed that IL8 and HMGB1 mRNA levels were significantly reduced in both treatment groups relative to control (Fig. 5C,D). Together, these data indicate that NKT attenuated oxidative stress and inflammatory gene expression in HKFs.

Discussion

The present study shows that nootkatone attenuates several activation-associated phenotypes in an SV40-immortalized human keloid fibroblast model. In the initial viability comparison, the SV40-immortalized HKF model appeared more sensitive to NKT than the SV40-immortalized HSF model, and the selected working concentrations were sufficient to alter multiple phenotypic readouts in HKFs. Across the functional, imaging, and transcriptional assays, the overall pattern was consistent with a shift away from the activated profibrotic state. Because HSFs were not

carried forward into downstream migration, invasion, immunofluorescence, ROS, or RT-qPCR assays, the present dataset cannot determine whether every downstream phenotype is keloid-selective rather than a broader dermal fibroblast response to NKT.

One prominent finding was the coordinated reduction in wound closure, Transwell invasion, cell elongation, actin organization, α-SMA intensity, and vinculin-positive focal adhesions. These readouts are biologically linked because actomyosin organization and focal adhesions together support traction generation, force transmission, and directional migration [13-16]. This is particularly relevant in keloid biology, in which fibroblasts exhibit abnormal mechanosensing and mechanoresponsive transcription. YAP/TAZ activation has been associated with keloid formation [24], keloid fibroblasts display elevated and dysfunctional mechanotransduction signaling even outside canonical TGF-β input [25], and recent studies have further implicated matrix stiffening-dependent nuclear mechanics, lysosomal remodeling, and Piezo1-YAP signaling in the invasive and matrix-producing phenotype of pathological scar fibroblasts [26-28]. In parallel, antifibrotic interventions that suppress integrin/FAK-associated signaling can reduce fibrosis-related outputs [29]. Because NKT also reduced viability, part of the decrease in wound closure and invasion may reflect reduced cell number or metabolic activity. However, the concordant changes in morphology, α-SMA, and focal adhesion abundance support an effect on the activated migratory/mechanoadaptive phenotype rather than a purely nonspecific cytotoxic response. Accordingly, the wound-closure and invasion data should be interpreted as anti-activation phenotypes rather than definitive motility-specific endpoints until proliferation-normalized or live-cell tracking experiments are performed.

NKT20 also reduced COL1A1, COL3A1, and FN1 mRNA, together with α-SMA immunofluorescence. These changes are relevant to keloid progression, in which persistent fibroblast activation, contractility, and matrix deposition form a feed-forward loop that increases tissue stiffness and further amplifies mechanosignaling [4-7,17,24-28]. Importantly, the ECM RT-qPCR data were obtained only for NKT20 under the current design; therefore, these results support suppression of ECM-related transcription at that dose but do not yet establish a full dose-response relationship. Nevertheless, the direction of effect is consistent with broader in vitro evidence that bioactive small molecules can coordinately modulate collagen-related output and fibroblast migration phenotypes [23].

Another important finding was the parallel reduction in intracellular ROS and in the inflammatory genes IL8 and HMGB1. Oxidative stress is increasingly implicated in keloid fibroblast activation and fibrotic remodeling [8-10]. Beyond generic ROS biology, keloid fibroblasts show hypoxia-associated metabolic reprogramming [30], GLUT1-linked enhancement of glycolysis and oxidative stress [31], and NOX4-dependent oxidative signaling downstream of TGF-β1 [32]. At the tissue level, keloids also exhibit evidence of oxidative damage together with altered Nrf2-related antioxidant responses [33]. Emerging work additionally links ferroptosis-related redox regulation to keloid fibroblast fibrosis [34]. Against this background, the reduction in DCFH-DA signal after NKT treatment is biologically

meaningful and supports the possibility that redox modulation is one component of the observed phenotypic restraint.

The decreases in HMGB1 and IL8 further suggest that NKT may dampen inflammatory amplification loops that cooperate with fibroblast activation. HMGB1 has been shown to promote keloid fibroblast migration and extracellular matrix-related activity through RAGE-MAPK and NF-κB signaling [35], and pharmacologic suppression of HMGB1-associated signaling can reduce collagen synthesis and enhance matrix-degrading activity in keloid models [36]. Recent work also supports a pathogenic role for IL-8/CXCL8-associated signaling in fibrotic skin disease [37], while keloid fibroblasts can upregulate CXCL8 in response to pro-inflammatory stimulation [38]. These observations fit well with prior reports that NKT exerts antioxidant and anti-inflammatory effects in neuroinflammation, liver injury, airway inflammation, and acute lung injury models [18-22]. The current study therefore extends NKT biology to human keloid fibroblasts and suggests several mechanistic directions for future work, including FAK/YAP/TAZ, Piezo1-associated calcium signaling, NOX4/Nrf2 balance, and HMGB1-RAGE/NF-κB-related pathways [24,25,28,32-35].

Several limitations should be acknowledged. First, the work was performed in vitro and does not recapitulate the full multicellular, vascular, immune, and mechanical microenvironment of keloid tissue. Second, both HKFs and HSFs were SV40-immortalized single-donor cell-line models; therefore, the findings may be influenced by donor background, immortalization-related changes, or culture adaptation and cannot be assumed to represent the full heterogeneity of primary keloid fibroblasts. Validation in primary, non-immortalized HKFs and HSFs from at least three independent donors is required to exclude donor-specific effects. Third, HSFs were included only in the viability screen, so the downstream functional and molecular effects should not be interpreted as definitively keloid-specific. Parallel HSF migration, invasion, cytoskeletal organization, focal-adhesion analysis, ROS measurement, and ECM/inflammatory gene-expression assays are needed to define disease selectivity. Fourth, because NKT reduced viability, additional migration-focused approaches--such as live-cell tracking, proliferation-normalized migration analysis, apoptosis assays, or matched cell-number conditions--would help distinguish antimigratory effects from antiproliferative or cytotoxic effects. Fifth, some image-based bulk fluorescence readouts, particularly field-level actin and ROS measurements, may be influenced by cell density and would benefit from per-cell normalization in future studies. Sixth, ECM-related readouts were evaluated mainly at the mRNA level, and COL1A1/COL3A1/FN1 were tested only in the NKT20 group. Protein-level validation, fuller dose-response analysis, and pathway-dissection experiments will be required to define the underlying mechanism more precisely. Even with these limitations, the convergence of the current assays supports an inhibitory effect of NKT on HKF activation-associated phenotypes.

Conclusions

Nootkatone attenuated multiple profibrotic features in an SV40-immortalized human keloid fibroblast model, including cell viability, wound closure, invasion, actin organization, α-SMA

immunofluorescence, focal adhesion abundance, intracellular ROS, and the mRNA expression of ECM- and inflammation-related genes. Under the conditions tested, ECM-related transcripts were reduced in the NKT20 group, whereas IL8 and HMGB1 were reduced in both NKT-treated groups. These findings support further mechanistic validation in primary, non-immortalized, multi-donor HKF/HSF models and translational keloid models.

References

[1] Boraldi F, Lofaro FD, Bonacorsi S, Mazzilli A, Garcia-Fernandez M, Quaglino D. The role of fibroblasts in skin homeostasis and repair. Biomedicines. 2024;12(7):1586. doi:10.3390/biomedicines12071586.

[2] Marella S, Plikus MV, Gudjonsson JE. Skin fibroblasts in health and disease: From extracellular matrix remodeling to immune regulation. J Invest Dermatol. 2026 Jan 5. doi:10.1016/j.jid.2025.12.002.

[3] Knoedler S, Broichhausen S, Guo R, Dai R, Knoedler L, Kauke-Navarro M, et al. Fibroblasts – the cellular choreographers of wound healing. Front Immunol. 2023;14:1233800. doi:10.3389/fimmu.2023.1233800.

[4] Ma Y, Liu Z, Miao L, Jiang X, Ruan H, Xuan R, Xu S. Mechanisms underlying pathological scarring by fibroblasts during wound healing. Int Wound J. 2023;20(6):2190-2206. doi:10.1111/iwj.14097.

[5] Fang X, Wang Y, Chen H, Yan Z, Jin S, Wu Y, Shu F, Xiao S. Hypertrophic scarring and keloids: Epidemiology, molecular pathogenesis, and therapeutic interventions. MedComm. 2025;6(10):e70381. doi:10.1002/mco2.70381.

[6] Zhang G, Liu Z, Li Z, Xu Y. Future directions about keloid scars based on pathogenesis and therapies. Clin Cosmet Investig Dermatol. 2024;17:2391-2408. doi:10.2147/CCID.S470650.

[7] Lei L, Lu Z. Advances in the characteristics of fibroblasts in keloid: A review. Exp Dermatol. 2026;35(3):e70222. doi:10.1111/exd.70222.

[8] Hong YK, Chang YH, Lin YC, Chen B, Guevara BEK, Hsu CK. Inflammation in wound healing and pathological scarring. Adv Wound Care (New Rochelle). 2023;12(5):288-300. doi:10.1089/wound.2021.0161.

[9] Makena P, Kikalova T, Prasad GL, Baxter SA. Oxidative stress and lung fibrosis: Towards an adverse outcome pathway. Int J Mol Sci. 2023;24(15):12490. doi:10.3390/ijms241512490.

[10] Whitcomb LA, Cao X, Thomas D, et al. Mitochondrial reactive oxygen species impact human fibroblast responses to protracted γ-ray exposures. Int J Radiat Biol. 2024;100(6):890-902. doi:10.1080/09553002.2024.2338518.

[11] Chen Y, Huang L, Gan RH, Yuan S, Lan T, Zheng D, Lu YG. IL-8 activates fibroblasts to promote the invasion of HNSCC cells via STAT3-MMP1. Cell Death Discov. 2024;10(1):65. doi:10.1038/s41420-024-01833-7.

[12] Yuan J, Mo Y, Zhang Y, Zhang Y, Zhang Q. HMGB1 derived from lung epithelial cells after cobalt nanoparticle exposure promotes the activation of lung fibroblasts. Nanotoxicology. 2024;18(6):565-581. doi:10.1080/17435390.2024.2404074.

[13] Yamaguchi N, Knaut H. Focal adhesion-mediated cell anchoring and migration: From in vitro to in vivo. Development. 2022;149(10):dev200647. doi:10.1242/dev.200647.

[14] Katsuta H, Sokabe M, Hirata H. From stress fiber to focal adhesion: A role of actin crosslinkers in force transmission. Front Cell Dev Biol. 2024;12:1444827. doi:10.3389/fcell.2024.1444827.

[15] Holland EN, Fernández-Yagüe MA, Zhou DW, O'Neill EB, Woodfolk AU, Mora-Boza A, Fu J, Schlaepfer DD, García AJ. FAK, vinculin, and talin control mechanosensitive YAP nuclear localization. Biomaterials. 2024;308:122542. doi:10.1016/j.biomaterials.2024.122542.

[16] Paddillaya N, et al. Substrate viscoelasticity regulates fibroblast adhesion and migration. Biointerphases. 2025;20(4):041010. doi:10.1116/6.0004585.

[17] Dong X, Xiang H, et al. Dermal fibroblast-derived extracellular matrix synergizes with keratinocytes in promoting re-epithelization and scarless healing of skin wounds: Towards optimized skin tissue engineering. Bioact Mater. 2025;47:1-17. doi:10.1016/j.bioactmat.2024.12.030.

[18] Park JE, Park JS, Leem YH, Kim DY, Kim HS. NQO1 mediates the anti-inflammatory effects of nootkatone in lipopolysaccharide-induced neuroinflammation by modulating the AMPK signaling pathway. Free Radic Biol Med. 2021;164:354-368. doi:10.1016/j.freeradbiomed.2021.01.015.

[19] Habotta OA, Abdeen A, Roomi AB, Elgndy AI, Sorour SM, et al. Nootkatone mitigated melamine-evoked hepatotoxicity by featuring oxidative stress and inflammation interconnected mechanisms: In vivo and in silico approaches. Toxics. 2023;11(9):784. doi:10.3390/toxics11090784.

[20] Dai C, Zhang X, Lin J, Shen J. Nootkatone supplementation ameliorates carbon tetrachloride-induced acute liver injury via the inhibition of oxidative stress, NF-κB pathways, and the activation of Nrf2/HO-1 pathway. Antioxidants (Basel). 2023;12(1):194. doi:10.3390/antiox12010194.

[21] Gai Y, Bai C, et al. Nootkatone attenuates airway inflammation in asthmatic mice through repressing ROS-induced NLRP3 inflammasome activation. Biochem Cell Biol. 2023;101(6):513-522. doi:10.1139/bcb-2023-0009.

[22] Hanuman DDV, Banothu AK, Bharani KK, Yadala RK, Khurana A, Gadige A, Gandham N. Nootkatone mitigates LPS-induced acute lung injury by modulating the NF-κB and Nrf2 pathways in mice. Front Vet Sci. 2025;12:1593919. doi:10.3389/fvets.2025.1593919.

[23] Jabłońska-Trypuć A, Pankiewicz W, Wołejko E, Sokołowska G, Estévez J, Sogorb MA, Wydro U. Human skin fibroblasts as an in vitro model illustrating changes in collagen levels and skin cell migration under the influence of selected plant hormones. Bioengineering (Basel). 2024;11(12):1188. doi:10.3390/bioengineering11121188.

[24] Aramaki-Hattori N, Okabe K, Hamada M, Takato T, Kishi K. Relationship between keloid formation and YAP/TAZ signaling. Plast Reconstr Surg Glob Open. 2017;5(6):e1357. doi:10.1097/GOX.0000000000001357.

[25] Deng Z, Subilia M, Chin IL, Hortin N, Stevenson AW, Wood FM, Prêle CM, Choi YS, Fear MW. Keloid fibroblasts have elevated and dysfunctional mechanotransduction signaling that is independent of TGF-β. J Dermatol Sci. 2021;104(1):11-20. doi:10.1016/j.jdermsci.2021.09.002.

[26] Fu X, Taghizadeh A, Taghizadeh M, Li CJ, Lim NK, Lee JH, Kim HS, Kim HW. Targeting nuclear mechanics mitigates the fibroblast invasiveness in pathological dermal scars induced by matrix stiffening. Adv Sci (Weinh). 2024;11(15):e2308253. doi:10.1002/advs.202308253.

[27] Ross R, Guo Y, Walker RN, Bergamaschi D, Shaw TJ, Connelly JT. Biomechanical activation of keloid fibroblasts promotes lysosomal remodeling and exocytosis. J Invest Dermatol. 2024;144(12):2730-2741. doi:10.1016/j.jid.2024.04.015.

[28] Liao C, Wang P, Zeng Q, Yan G, Gao J, Liu J, Yan J, Wang X. Piezo1-mediated calcium flux transfers mechanosignal to YAP to stimulate matrix production in keloid. J Invest Dermatol. 2025;145(11):2869-2881.e9. doi:10.1016/j.jid.2025.03.039.

[29] Chen Y, Gong Y, Shi M, Zhu H, Tang Y, Huang D, Wang W, Shi C, Xia X, Zhang Y, et al. miR-3606-3p alleviates skin fibrosis by integratively suppressing the integrin/FAK, p-AKT/p-ERK, and TGF-β signaling cascades. J Adv Res. 2025;75:271-290. doi:10.1016/j.jare.2024.11.027.

[30] Wang Q, Wang P, Qin Z, Yang X, Pan B, Nie F, Bi H. Altered glucose metabolism and cell function in keloid fibroblasts under hypoxia. Redox Biol. 2021;38:101815. doi:10.1016/j.redox.2020.101815.

[31] Lu YY, Wu CH, Hong CH, Chang KL, Lee CH. GLUT-1 enhances glycolysis, oxidative stress, and fibroblast proliferation in keloid. Life (Basel). 2021;11(6):505. doi:10.3390/life11060505.

[32] Qin H, Zhang L, Li M, Liu Y, Sun S, Nie W, Bai B, Li G, Zhang G. EGR1/NOX4 pathway regulates oxidative stress and further facilitates fibrosis progression in keloids responses to TGF-β1. J Dermatol Sci. 2022;108(1):138-145. doi:10.1016/j.jdermsci.2022.12.009.

[33] Lee YJ, Kwon SB, Kim CH, Cho HD, Nam HS, Lee SH, Lee MW, Nam DH, Choi CY, Cho MK. Oxidative damage and nuclear factor erythroid 2-related factor 2 protein expression in normal skin and keloid tissue. Ann Dermatol. 2015;27(5):507-516. doi:10.5021/ad.2015.27.5.507.

[34] Yang L, Li X, Wang Y. Ferrostatin-1 inhibits fibroblast fibrosis in keloid by inhibiting ferroptosis. PeerJ. 2024;12:e17551. doi:10.7717/peerj.17551.

[35] Kim J, Park JC, Lee MH, Yang CE, Lee JH, Lee WJ. High-mobility group box 1 mediates fibroblast activity via RAGE-MAPK and NF-κB signaling in keloid scar formation. Int J Mol Sci. 2018;19(1):76. doi:10.3390/ijms19010076.

[36] Baek W, Park S, Lee Y, Roh H, Yun CO, Roh TS, Lee WJ. Ethyl pyruvate decreases collagen synthesis and upregulates MMP activity in keloid fibroblasts and keloid spheroids. Int J Mol Sci. 2024;25(11):5844. doi:10.3390/ijms25115844.

[37] Zhang W, Peng Q, Huang X, Huang Q, Zhang Z, Li F, et al. Commensal microbiome dysbiosis elicits interleukin-8 signaling to drive fibrotic skin disease. PNAS Nexus. 2024;3(7):pgae273. doi:10.1093/pnasnexus/pgae273.

[38] Chen Y, Xu Y, Zhang J, Feng C, Chen J, Song Y, Pan J, Zhu J, Cheng H. Glutamate enhances the production of inflammatory cytokines IL-6 and IL-11, as well as chemokines CXCL2, CXCL3, and CXCL8 in keloid fibroblasts. Front Mol Biosci. 2026;12:1720876. doi:10.3389/fmolb.2025.1720876.

Figure Legends

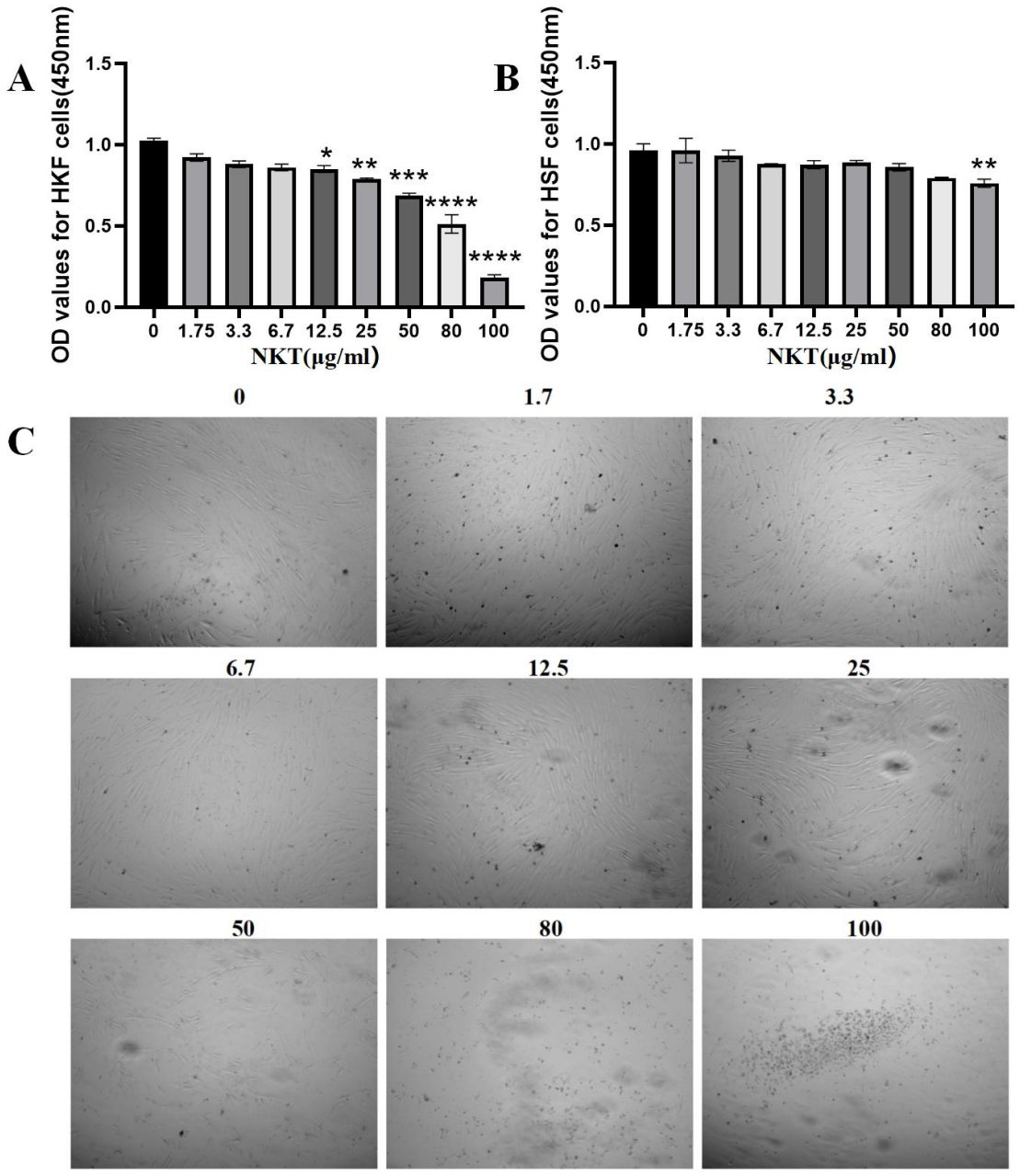

Figure 1. Concentration-dependent effects of nootkatone on SV40-immortalized fibroblast viability and HKF morphology. (A) CCK-8 assay of HKF viability after exposure to the indicated concentrations of nootkatone. (B) CCK-8 assay of HSF viability over the same concentration range. (C) Representative phase-contrast images of HKFs exposed to increasing concentrations of nootkatone. Statistical annotations are presented as shown in the original figure. * $P < 0.05$, ** $P < 0.01$, *** $P < 0.001$, **** $P < 0.0001$.

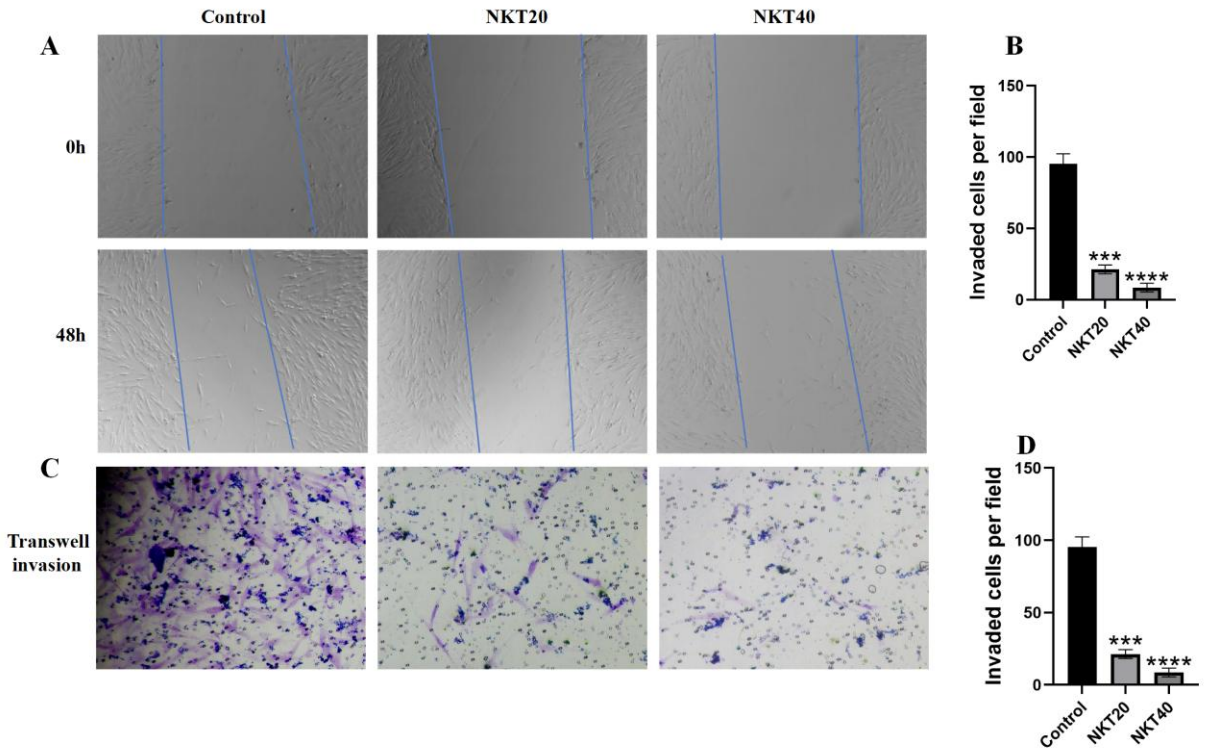

Figure 2. Nootkatone reduces scratch-wound closure and Transwell invasion of HKFs. (A) Representative scratch-wound images obtained at 0 and 48 h in the control, NKT20, and NKT40 groups. Blue lines delineate the wound margins. (B) Quantification of wound closure in the scratch assay. (C) Representative images of invaded HKFs in the Transwell assay. (D) Quantification of invaded cells per field.* $P < 0.05$, **$P < 0.01$, *** $P < 0.001$， ****$P < 0.0001$.

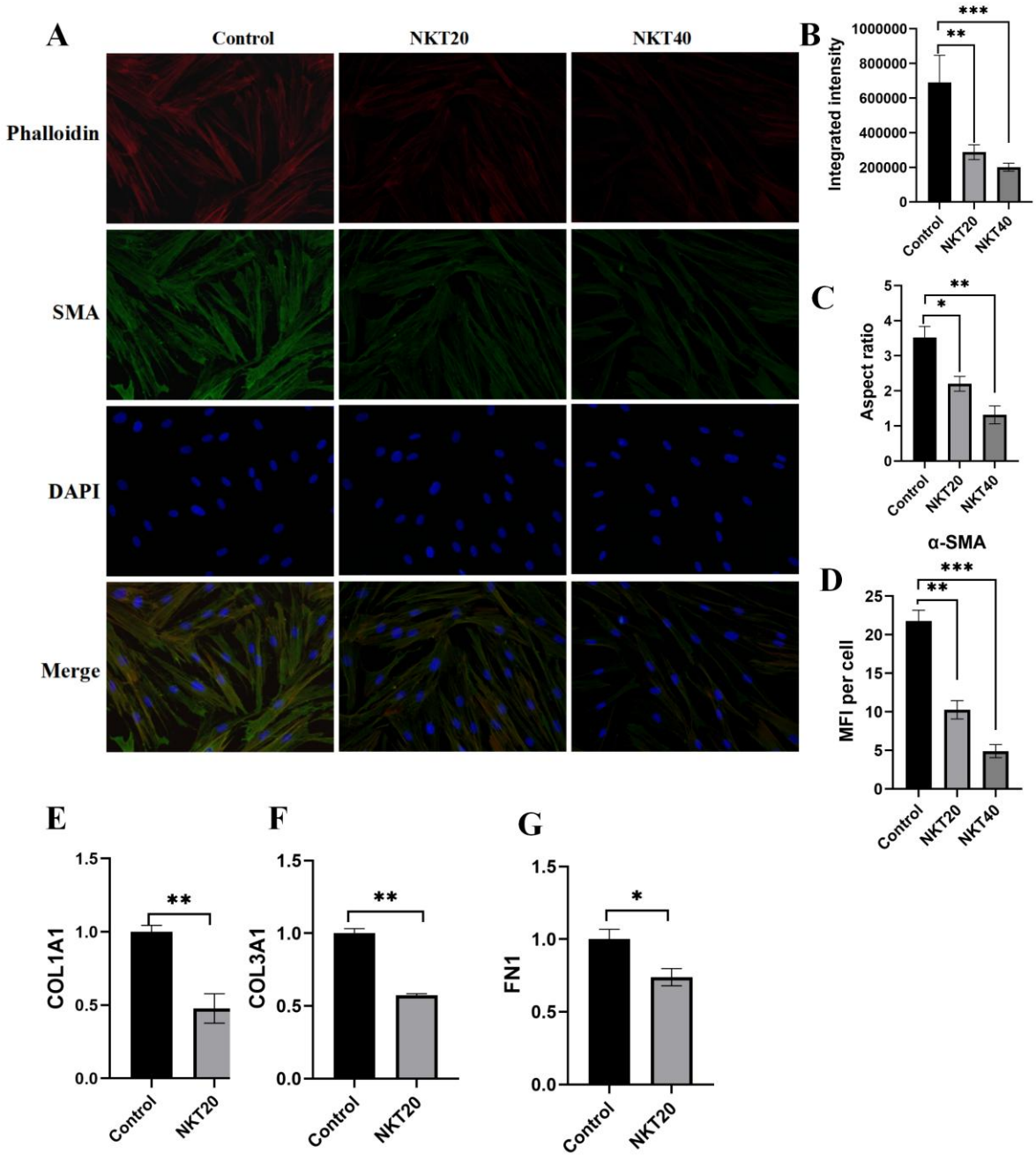

Figure 3. Nootkatone attenuates actin organization, α-SMA immunofluorescence, and ECM-related gene expression in SV40-immortalized HKFs. (A) Representative immunofluorescence images of phalloidin (red), α-SMA (green), DAPI (blue), and merged images in the control, NKT20, and NKT40 groups. (B) Quantification of integrated phalloidin intensity. (C) Quantification of cell aspect ratio. (D) Quantification of α-SMA mean fluorescence intensity (MFI) per cell. (E-G) Relative mRNA expression of COL1A1, COL3A1, and FN1 in the control and NKT20 groups. Comparative immunofluorescence images were acquired under identical

exposure settings and processed uniformly across groups. * P < 0.05, **P < 0.01, *** P < 0.001, ****P < 0.0001.

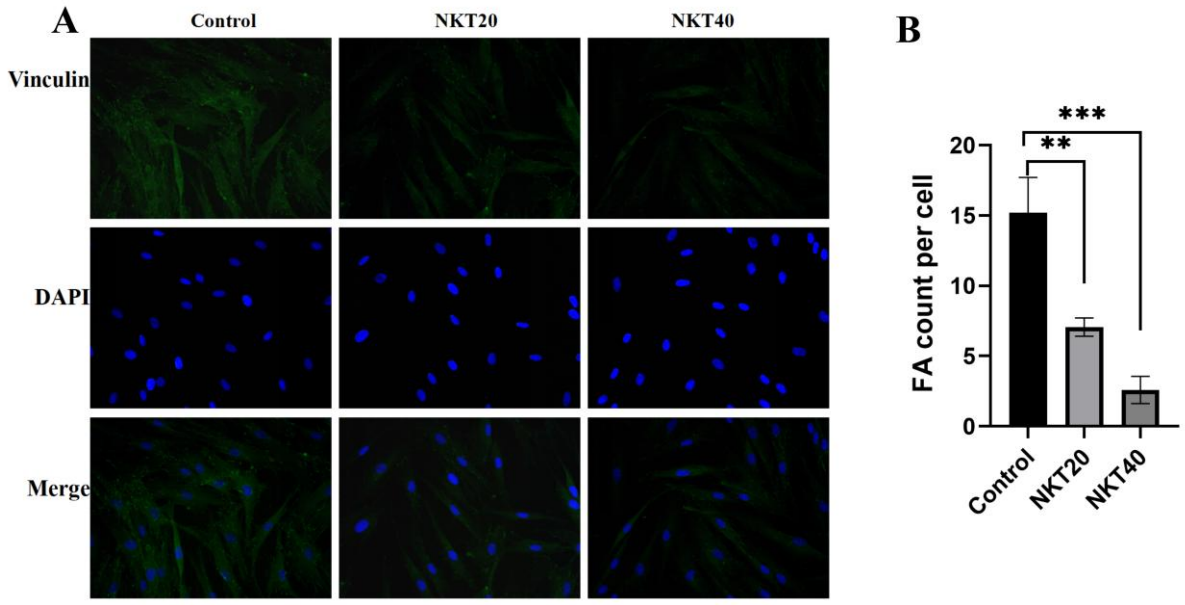

Figure 4. Nootkatone reduces vinculin-positive focal adhesion abundance in SV40-immortalized HKFs. (A) Representative immunofluorescence images of vinculin (green), DAPI (blue), and merged images in the control, NKT20, and NKT40 groups. (B) Quantification of focal adhesion counts per cell. Comparative immunofluorescence images were acquired under identical exposure settings and processed uniformly across groups. * P < 0.05, **P < 0.01, *** P < 0.001, ****P < 0.0001.

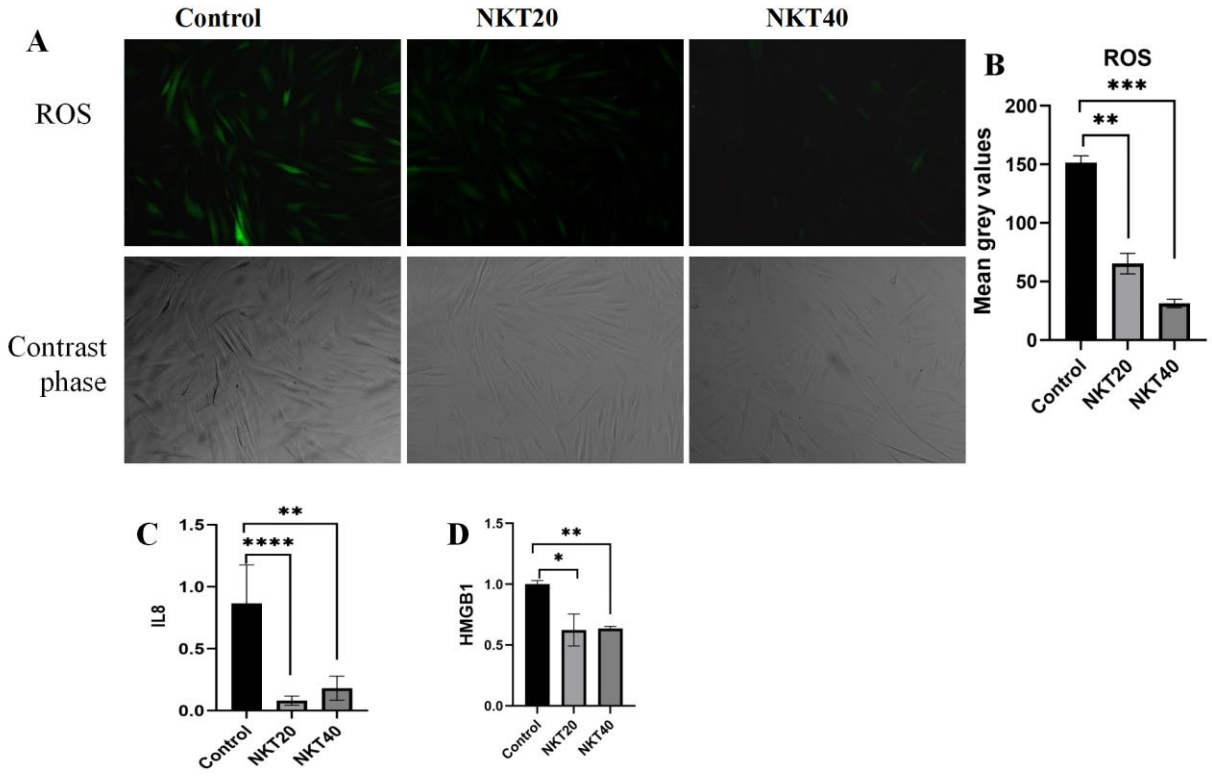

Figure 5. Nootkatone lowers intracellular ROS levels and inflammatory gene expression. (A) Representative DCFH-DA fluorescence images and corresponding phase-contrast images in the control, NKT20, and NKT40 groups. (B) Quantification of ROS signal as mean gray value. (C) Relative IL8 mRNA expression. (D) Relative HMGB1 mRNA expression.* $P < 0.05$, **$P < 0.01$, *** $P < 0.001$， ****$P < 0.0001$.